Proceedings of
10th European Conference on Turbomachinery Fluid dynamics & Thermodynamics
ETC10, April 15-19, 2013, Lappeenranta, Finland

INFLUENCE OF REGENERATION-INDUCED VARIANCES OF STATOR VANES ON THE VIBRATION BEHAVIOUR OF ROTOR BLADES IN AXIAL TURBINES

J. Aschenbruck - C.E. Meinzer - J.R. Seume

Institute of Turbomachinery and Fluid Dynamics (TFD), Leibniz Universitaet Hannover,
Hannover, Germany, aschenbruck@tfd.uni-hannover.de

ABSTRACT

The regeneration of highly loaded turbine blades causes variances in geometrical parameters. To determine such typical, regeneration-induced variances of turbine blades, refurbished blades of aircraft jet-engines are analysed and significant variations of different geometrical parameters are identified. These characteristic variances are applied to stator vanes of the investigated turbine stage.

In the next step, steady-flow CFD simulations are performed with these varied vanes to evaluate the effects of geometric variances on their aerodynamic performance. This analysis indicates a high influence on the total pressure-loss coefficient of the varied vanes. The variation of the trailing-edge thickness, the blade thickness, and the variation of the chord length have effects of comparable magnitudes. Based on these results, the influence of the trailing-edge variation on the low engine-order excitation is investigated using a forced response analysis. It is shown, that the vibration amplitudes of some modes are significantly higher due to the geometrical variation.

NOMENCLATURE

c	chord length	mm	r	stage reaction	$-$
c_{ax}	axial chord length	mm	s	pitch	mm
k	reduced frequency	$-$	t_{bl}	blade thickness	mm
$\dot{m}$	mass flow	$\frac{kg}{s}$	t_{TE}	trailing-edge thickness	mm
Ma	mach number	$-$	β_{ex}	outlet flow angle	$^\circ$
n	revolution	rpm	λ	stagger angle	$^\circ$
p_{st}	static pressure	Pa	Ψ	loading coefficient	$-$
p_{tot}	total pressure	Pa	ζ	total pressure-loss coefficient	$-$

INTRODUCTION

Turbine blades are the most aerodynamically, mechanically, and thermally loaded parts in aircraft gas turbine engines. The thermal and mechanical loads acting on the blades cause substantial wear. As a consequence, blades must be refurbished regularly. Depending on the condition of the blade, different repair methods exist which vary with respect to the accuracy of restoring the worn contour. Thus, the geometry of the affected blades varies after regeneration. The first objective of this paper is to develop a method for quantifying the occurring variations. Lange et al. (2008) describe such a method for compressor blades. Their method indicates geometrical deviations induced by manufacturing tolerances.

In the next step of the present paper, the influence of the geometric variances on the aerodynamic of the blades is investigated using CFD simulations. For the investigations, the variances are transferred to one stage of a model air turbine. The aerodynamic influence of manufacturing tolerances

on the performance of turbines were experimentally explored early on by Bammert and Sandstede (1976) who found a lower efficiency due to higher blade thickness. Recently, numerical investigations of these effect are done by Goulos et al. (2009) and Zachos and Kalfas (2010). Torre et al. (2012) also conducted experimental work on the influence of blade thickness deviation on the efficiency of low-pressure turbines. The deviations were applied at the pressure side of the blade and it is shown that these variations have no influence on the efficiency.

The main objective of the present paper is to investigate the effect of regeneration-induced variances of stator vanes on the low engine-order (LEO) excitation of the rotor. The focus is set on the excitation of low eigenfrequencies, because this would significantly shorten the operating life of rotor blades. Bréard et al. (2003) show in a numeric study that the influence of unknown variability in the blading on the LEO excitation is non neglectable. Damages of several stator vanes can also excite the LEO as presented in Di Mare et al. (2007) and Meyer et al. (2011). These results are also confirmed by numerical and experimental investigations from Petrov et al. (2010) using a full chain for the predictive forced response.

DETERMINATION OF REGENERATION-INDUCED VARIANCES

To determine geometrical variances of turbine blades caused by wear and regeneration, at first, a suitable method needs to be developed to classify geometric variations of flow-related parameters. Then, these variations can be investigated by comparing refurbished blades with the original CAD-model of the blade. In the following section, the methodology developed to determine regeneration-induced variances is presented and then applied on the analysis of twenty turbine blades of a real aircraft engine.

Methodology

The methodology is developed to quantify the variances of refurbished turbine blades in comparison to the original geometry of the blade. The focus is set to geometric parameters, which affect the aerodynamic and aeroelastic behaviour of the blades. The different steps of this method are depicted in Fig. 1.

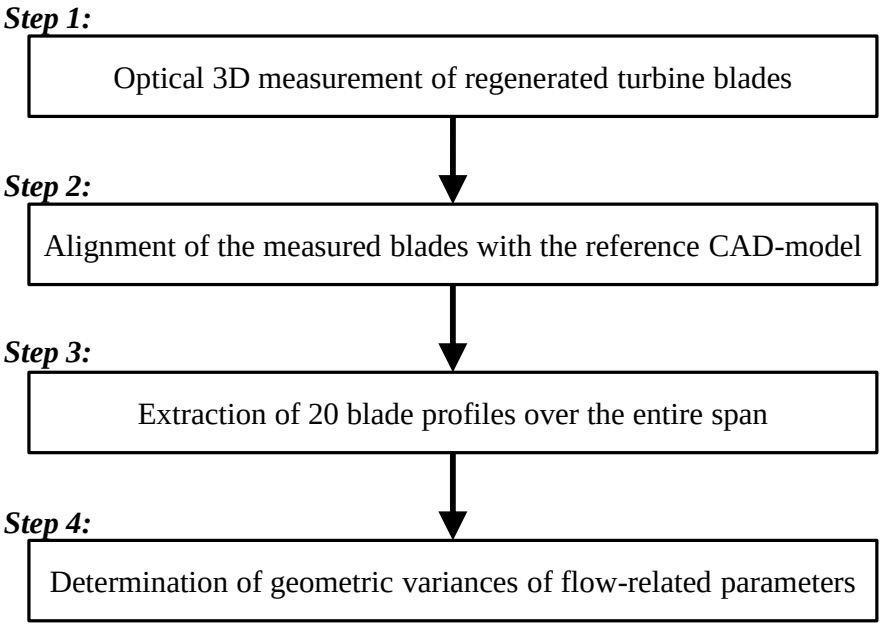

Figure 1: Overview of the method to determine geometric deviations of turbine blades

First, the surface of the refurbished turbine blades is measured using a three-dimensional optical scanner (GOM TripleScanII), which has an accuracy of 0.01 mm and takes measurements as closely spaced as 0.13 mm. Optical scanners have the advantage that only a short time, compared with tactile measurements systems, is needed for measuring the entire blade. After the measurement, the geometries of the blades are available as point clouds. In the next step (see Fig. 1, step 2), the measured blades have to be aligned with the reference CAD-model, because the coordinate system of the measured blades and of the reference model are not identical. For this step, the program GOM Inspect (V7.5) is used, which aligns the blades using a best-fit algorithm in the region where the blade is fixed to the rotor disk or the casing (e.g. blade root, shroud band).

The third step is to extract a previously defined number of radial blade profiles. These profiles are exported equally spaced over the entire blade span for all measured blades. In the present study, 400 profiles of twenty refurbished blades (twenty of each blade) are compared with the reference geometry.

In the final step (see Fig. 1, step 4), the geometric deviations of flow-related parameters are extracted from the exported profiles. For this purpose, a Matlab tool is implemented, which first reads in the profiles and generates the chamber line for each profile. After that, the thickness distribution over the axial chord length is determined with respect to the previously defined chamber line. Furthermore, the tool is able to calculate the axial chord length c_{ax} and the stagger angle λ. The leading and trailing-edge thickness is determined by fitting circles to the points that define the leading and trailing-edge region. After the determination of the geometric parameters of the blade profiles, they are compared with the reference geometry.

Interpretation of the variances

Four geometric parameters are compared with the CAD geometry of the blade and the deviations from the design geometry induced by regeneration are evaluated. These parameters are

- the axial chord length c_{ax},
- the stagger angle λ,
- the blade thickness t_{bl}, and
- the thickness of the trailing-edge t_{TE}.

The detected deviations are interpreted using two bar charts for every parameter (see Figures 2 - 5). In the left bar chart, the standard deviation of all 400 profiles blades is plotted and the deviation of five exemplary blade profiles at 85$\%$ span is depicted for visualization. These five exemplary profiles are identical for all four parameters. Additionally, the error bars of the deviations are plotted considering the maximum error due to the accuracy of the optical scanner and the calculation of the parameters. The right bar chart illustrates the percentage distribution of the deviations occurring.

The evaluation of the axial chord length deviation is depicted in Fig. 2. For all profiles compared here, the standard deviation is about 0.83$\%$ of the reference axial chord length. Compared with that, the five blade profiles plotted in Fig. 2 (a) have deviations between -1,45$\%$ and -0,96$\%$. Figure 2 (b) illustrates the percentage distributions of axial chord length deviation. The distribution is shifted to the negative side. Meaning that wear during operation and the regeneration process cause shorter axial chord lengths.

In Figure 3, the deviation of the stagger angle is analysed. The standard deviation for all 400 cases is about 0.33° (see Fig. 3 a). The deviations of the five blade profiles plotted here are positive and between 0.15° and 0.76°. This result confirms the percentage distribution of the stagger angle, which is depicted in Fig. 3 (b). Only 6.5$\%$ of the investigated profiles have a negative deviation of the stagger angle. Consequently, the distribution of the deviation is shifted to the positive side.

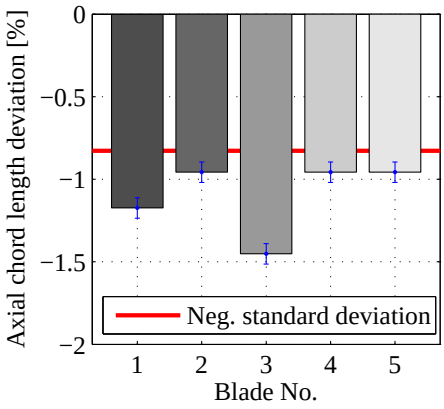

(a) Deviation of the axial chord length of 5 blades at 85% span

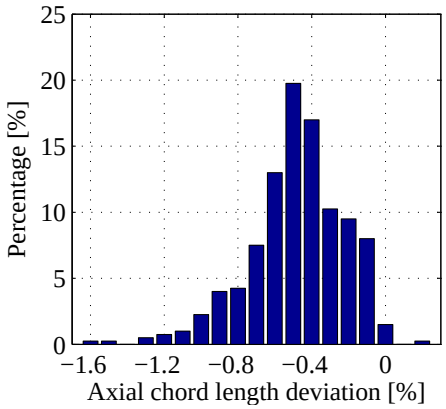

(b) Percentage distribution of the axial chord length deviation

Figure 2: Deviations of the axial chord length of refurbished turbine blades compared with the design geometry

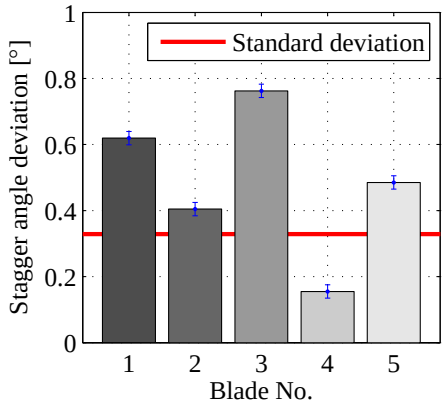

(a) Deviation of the stagger angle λ of 5 blades at 85% span

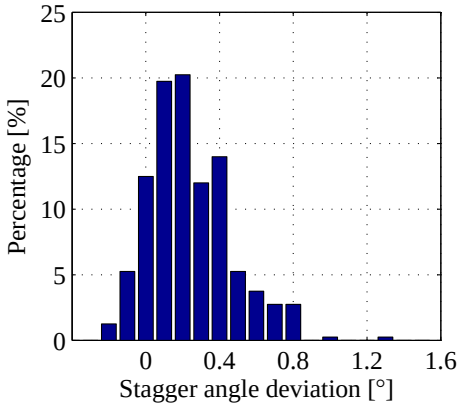

(b) Percentage distribution of the stagger angle deviation

Figure 3: Deviations of the stagger angle of refurbished turbine blades compared with the design geometry

Two more geometric parameters, the blade thickness and the thickness of the trailing-edge, are investigated. The deviation of the blade thickness is determined over the axial chord length of each profile. For the evaluation, the maximum value of the thickness deviation is selected in the range of 10% to 90% of the axial chord length c_{ax}. Then, the maximum deviation is normalized by the maximum thickness of the reference blade profile. In Fig. 4 (a), the standard deviation of the thickness deviation is plotted. It is about 2.8%. The maximum deviation is about 7%, which is more than twice the standard deviation (see Fig. 4 b). The distribution of the thickness deviation is shifted to the negative side, which was already the case for the axial chord length. This is caused by wear and regeneration process.

Finally, the deviation of the trailing-edge is investigated and depicted in Fig. 5. Because of the thin trailing-edge, the percentage deviation is higher compared to the other parameter. Again, most of the deviations are negative. Approximately 90% of the trailing-edges have a negative deviation (see Fig. 5 b). The maximum deviation of the trailing-edge is about 50% of the reference trailing-edge thickness and the standard deviation is 19.4%. The comparison of the deviation of the trailing-edge and the blade profile shows different trends for the same blade profiles (see Fig. 4 (a) and Fig. 5 (a), blade No. 4 and 5). Accordingly, there is no correlation between the deviation of the trailing-edge thickness and the thickness of the blade.

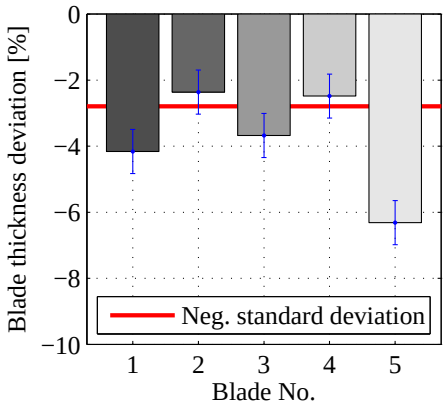

(a) Maximum deviation of the blade profile thickness of 5 blades at 85% span

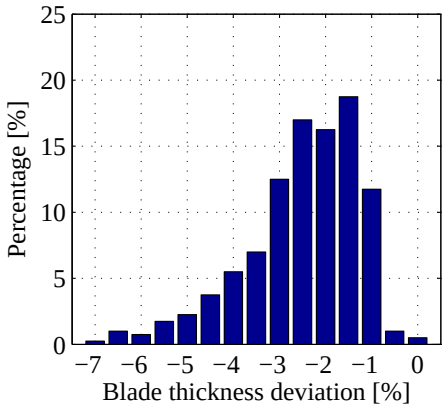

(b) Percentage distribution of the blade thickness deviation

Figure 4: Maximum deviations of the blade profile thickness of refurbished turbine blades compared with the design geometry

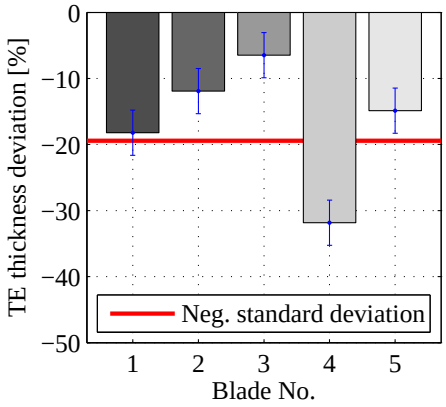

(a) Deviation of the trailing-edge thickness of 5 blades at 85% span

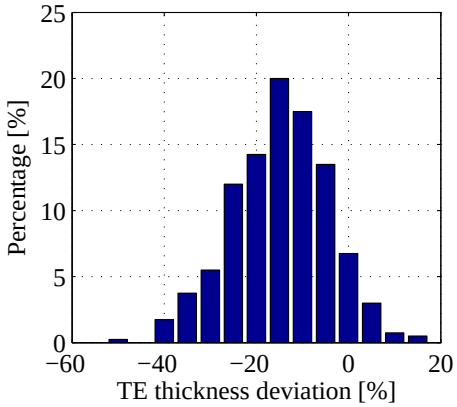

(b) Percentaged distribution of the trailing-edge thickness deviation

Figure 5: Deviations of the trailing-edge thickness of refurbished turbine blades compared with the design geometry

AERODYNAMIC ANALYSIS OF THE VARIANCES

The regeneration-induced variances discussed above are derived from refurbished turbine blades of a jet engine. These variances are now transferred to the blades of the model air-turbine at the Institute of Turbomachinery and Fluid Dynamics. In the present paper, the four different types of geometry variations are simulated in CFD and their influence on the aerodynamics is determined prior to conducting the experimental work.

Test-configuration

For the aerodynamic and aeroelastic investigation, the fifth and last stage of the axial air-turbine is used. In Figure 6, two passages of the vane and blade of this stage are shown. The blades of this stage are thinner and longer compared to the blades of the four preceding stages. This causes a higher sensitivity for vibrations. Further details of this stage are listed in Table 1.

Impact of the geometric variances on the aerodynamic

The variances determined are transferred to the vane of the fifth stage of the air-turbine. As in the preceding section, the four geometric parameters are investigated with respect to the aerodynamic

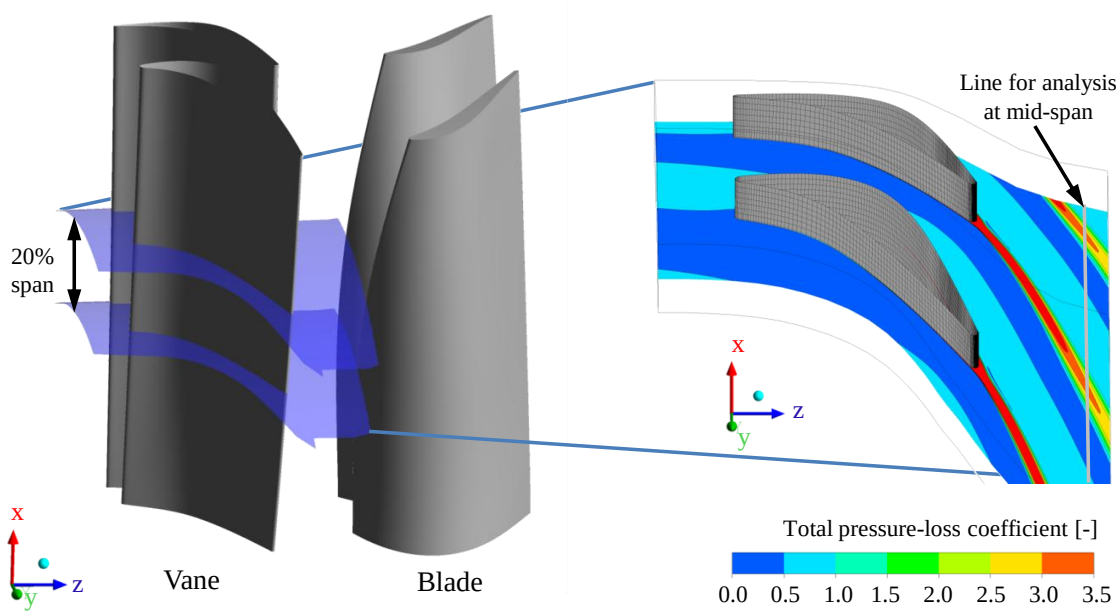

Figure 6: Fifth stage of the axial air turbine and the section of the vane passage for the aerodynamic investigations

Table 1: Parameters of the fifth stage of the axial air-turbine

Number of vanes	29
Number of blades	30
rated mass flow $\dot{m}$	8,5 $\frac{kg}{s}$
rated revolutions n	7500 rpm
span of the blade	108 mm
mach number Ma_{in}	0.145
mach number Ma_{ex}	0.325
reduced frequency k **of the blade**	1.2
loading coefficient Ψ	0.7
stage reaction r	0.2

influence. The range of these parameters is selected considering the results derived from the measured jet engine blades.

For all geometric parameters, at least four varied vanes are created and then simulated with steady CFD. For these simulations, twenty percent of the mid-span of the vanes are modelled, as depicted in the right part of Fig. 6. The rotor blade was not simulated for these investigations. This simplification reduces the computing time. As the variations are constant over the entire span, the flow will still be captured with high accuracy. The block-structured grid for the passage consists of approximately 600,000 nodes. For the aerodynamic analysis, the vane is modelled without the downstream rotor blade in order to analyse the wake without the blockage of the rotor blade. The wake is evaluated using the total pressure-loss coefficient

$$\zeta = \frac{p_{tot,0} - p_{tot}}{p_{tot,0} - p_{st,0}}, \tag{1}$$

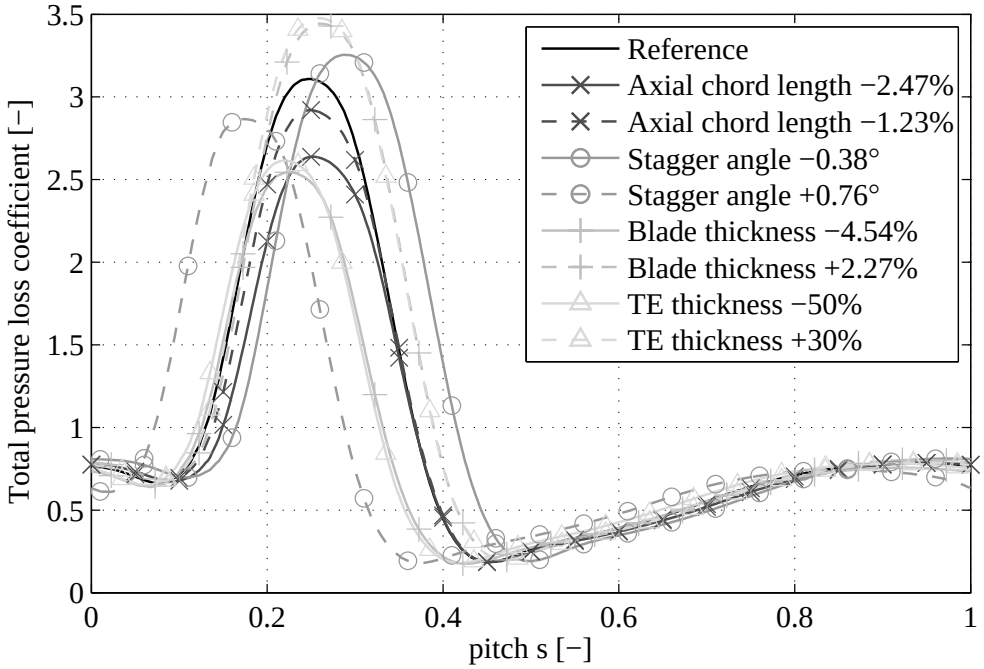

Figure 7: Total pressure-loss coefficient of the wakes of the varied vanes

the static pressure p_{st}, and the outlet flow angle β_{ex}. These parameters are analysed on the mid-span line of the passage (see Fig. 6). This line is located at the axial position of the leading edge of the blade.

In Figure 7, the total pressure-loss coefficient ζ of the vane wake is plotted over the normalized pitch s. For each geometrical parameter, the results of two varied geometries are shown. The values of these variations are in accordance with the determined variations of the jet-engine turbine blades presented in the preceding section. The wake of the reference geometry is located at a pitch s of 0.25 and has a maximum pressure-loss coefficient ζ of 3.1. The comparison of the graphs of the varied geometries shows significant differences in the wake amplitude and in the pitch position of the wake. These deviations depend on the variation of the blade. A negative deviation of the axial chord length reduces the total pressure-loss coefficient ζ of the wake. The circumferential position of the wake is not influenced. Thus, the outflow angle is similar to that of the reference. In contrast to this, the variation of the stagger angle influences the wake position significantly, but has a smaller effect on the total pressure-loss coefficient ζ. The thickness variation of the trailing-edge and of the blade profile has a similar impact on the total pressure-loss coefficient ζ. Especially the total pressure-loss coefficient of the negative variations is almost identical.

The results of all three aerodynamic parameters are summarized in Fig. 8. The deviations of these parameters are shown in three diagrams depending on the occurring maximum and minimum variation. For all three aerodynamic parameters the deviation is compared to the reference parameters. In the left diagram of Fig. 8, the deviation of the maximum value of the total pressure-loss coefficient is plotted. The results of this diagram are in line with those in Fig. 7, i.e. the variation of the axial chord length, of the blade, and of trailing-edge thickness have almost the same impact. The deviation of the total pressure-loss coefficient is about -0.5.

The static pressure p_{st} is integrated circumferentially over the mid-span of the passage. For all geometric variations, the values of the maximum deviations are less than $10\ Pa$. These deviations are negligible compared to the deviation of the total pressure. Finally, the deviation of the outlet

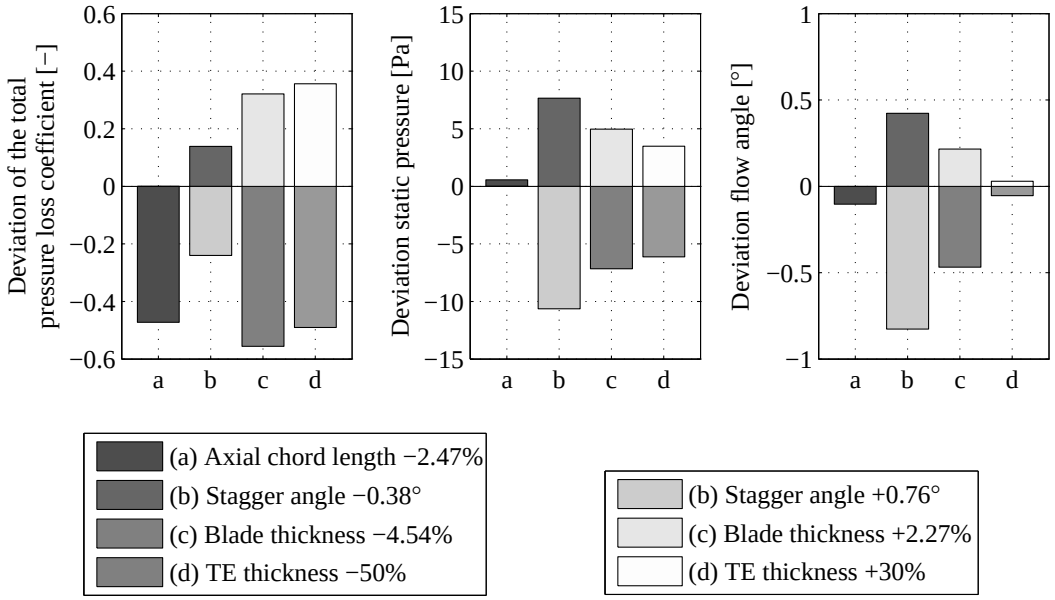

Figure 8: Influence of the geometric variations on aerodynamic parameters

flow angle is determined. The flow angle β_{ex} is also integrated over the mid-span. Compared to the total pressure-loss coefficient, the influence of the geometric parameters differs. The variations of the stagger angle significantly affect the flow angle. By contrast, the variations of the axial chord length as well as the variations of the trailing-edge thickness are negligible.

Overall, the determined variations of the real turbine blades have a significant influence on the total pressure-loss coefficient ζ and the flow angle β_{ex}. The above analysis indicates almost the same influence of the variation of the trailing-edge thickness, the blade thickness, and the variation of the chord length. For this reason, one of these three parameters, the trailing-edge thickness, is selected for the force response analysis in the following section.

FORCED RESPONSE ANALYSIS

The numerical modeling of aeroelastic phenomena combines two fields of mechanical engineering structural dynamics and fluid dynamics. Hence, it requires a multidisciplinary approach to link the tools and methods commonly used in these fields. This is either done using available multiphysics coupling codes or custom scripts that couple the specific finite volume and finite element codes used for the fluid and structural computations.

One challenge is to find an adequate modeling depth for coupling, which on the one hand retains the fundamental features of the problem and on the other hand leads to a problem that can be solved with the available amount of time and resources. The two principal approaches in coupling the fluid and the structural domain can be differentiated into bi-directional and uni-directional fluid-structure interaction (FSI). The bi-directional FSI returns the flow-induced deformation of the structural model to the CFD and updates the flow path at every iteration. In the unidirectional FSI this feedback loop remains open, thus, reducing the computational effort. This is one reason why this decoupled approach is commonly used today (Meyer et al., 2011). Due to the high mass ratios found in turbomachines the unsteady aerodynamic loads are usually not able to shift the frequency of the blade (Förstching, 1994), thus the decoupled approach is a valid simplification.

In practice, various methods for uni-directional load transfer exist. Traupel (1982) proposes the excitation of the blade by applying an oscillating spot load. The magnitude of this load is given by

the stimulus, which is defined as the ratio amplitude of the fluctuating total pressure at a frequency of interest to the average total pressure. According to Traupel (1982), the stimulus will be of the order of 5 to 10%. A more detailed load transfer can be achieved by perturbing the static pressure distribution on the blade surface as done e.g. by Henke et al. (2008). A comparison of spot loads applied along the local centers of gravity of different span sections to a corresponding time series of surface pressures mapped onto the FE model is given by Drewczynski et al. (2012). Both studies emphasize the more detailed load transfer when surface pressure mapping is used. However, this requires a higher computational effort. A comprehensive insight to forced response analysis is given by Chiang and Kielb (1993).

Method

In order to further reduce the resources needed for computing the structural solution by means of a transient analysis, a different approach is employed in the present study (c.f. Fig. 9). The oscillating pressure loads acting on the blade surface are Fourier transformed, filtered, and applied as a complex surface load to a harmonic response analysis (Fig. 10).

Forced response refers to the excitation of blades at discrete frequencies synchronous with integer multiples of the rotational frequency. Hence, the excitation pattern in the time domain can be represented with some accuracy by just retaining the complex pressures for the most dominant harmonics of the blade passing frequency (BPF). This process first solves the unsteady flow problem and then excites the structural model with the derived loads as will be discussed in some detail below.

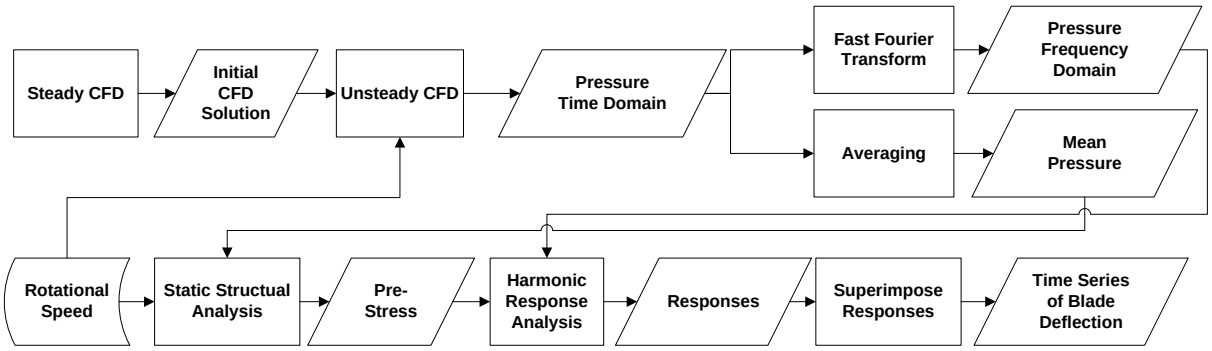

Figure 9: Flow chart of the present unidirectional FSI approach using the harmonic response analysis.

Unsteady CFD Solution

The unsteady flow problem is solved for the fifth stage only, omitting multi-stage effects in the forced-response analysis. The frozen-rotor initial solution which is needed for the unsteady CFD is preceded by a mixing plane CFD simulation of the whole turbine to establish correct inflow conditions. The stator vane is meshed as to resolve near-wall flows ($\max(y^+) \approx 1$) and the wake region, while the rotor is meshed with a uniform grid over the whole passage. This allows the stator wakes to propagate well into the rotor domain. Edge lengths at the stator-rotor interface are about the size of the smallest edge in the stator wake region. For the rotor a $\max(y^+) \approx 34$ is used.

The nominal operating point at a rotational speed of 7500 rpm and a mass flow of 8.5 kg/s is simulated for both the reference case and the variance case using a time step of $4.16671 \cdot 10^{-6}$ s. The SST model is used for turbulence and the Gamma-Theta model for transition modelling on the stator. For the frame change, the ANSYS Transient-Rotor-Stator model is utilized in the unsteady CFD and the frozen rotor model for the initial solution. Instead of the original 29 stator vanes / 30 rotor blades configuration, the variance case is modeled as two passages using scaled stator vanes to match a 24° sector. So two alternating stator vanes are succeeded by two identical rotor blades (see Fig. 6).

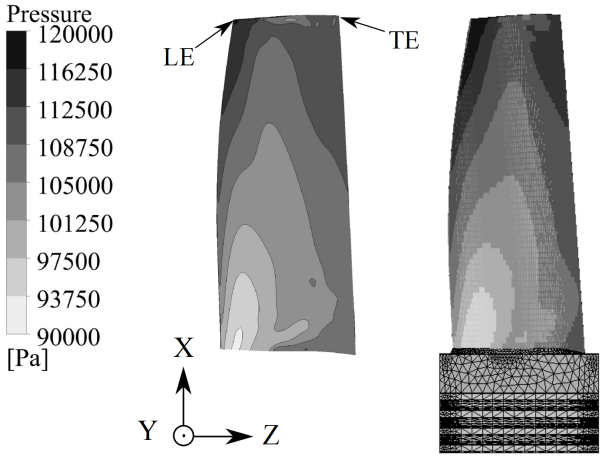

Figure 10: Mean pressure from CFD (left) mapped onto FE surface mesh (right).

Along with the CFD simulations a discretisation study for spatial and temporal resolution is conducted to ensure accurate modelling of the flow field and the efficient use of computational resources. After a converged unsteady solution is reached, the surface pressure on the rotor blade is exported for each time step and mapped onto the FE grid using the mapping feature of ANSYS CFD-Post.

Harmonic Analysis

The oscillating surfaces pressures from the preceding unsteady flow simulation could now be fed directly into a transient structural analysis. This would require a long time series since transient effect would have to settle down before a steady response is reached. The resources needed to obtain such a long time series signal from the CFD simulation are excessively high. Therefore, the highly periodic character of turbomachinery flow is exploited by transforming the surface pressures to frequency domain and further reducing the data by filtering all but the frequencies of interest. After that a harmonic response analysis is performed instead of a transient structural analysis.

A harmonic response analysis (Eq. 2) solves for the steady-state response of a structure which is exposed to a harmonic load:

$$M\ddot{x} + D\dot{x} + Kx = \hat{F}\sin(\omega t) \tag{2}$$

If additional steady forces act on the structure, this pre-stress can be considered in an earlier static analysis. For the present study the first three harmonics of the BPF are retained in the excitation for

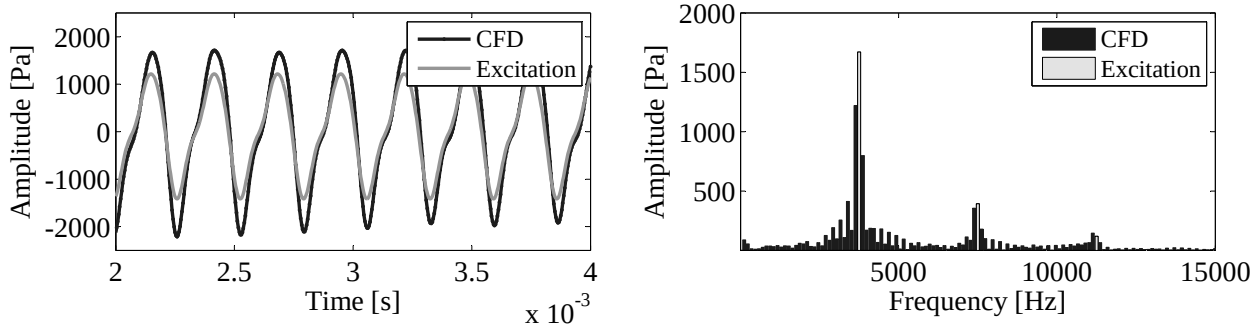

Figure 11: Unsteady pressure from CFD and excitation with three harmonics of BPF retained.

forced response analysis (c.f. Fig. 11). This already captures the basic features of the time signal. After performing a separate analysis for each frequency of interest, the resulting responses can be superimposed and reassembled to a time series. In the present study, the focus is set on excitation by

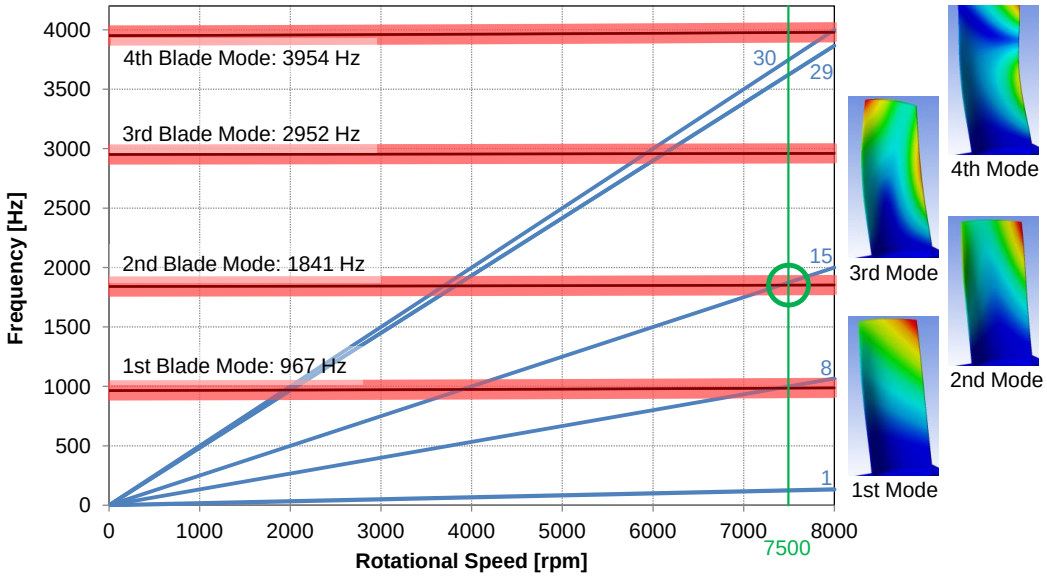

Figure 12: Campbell diagram and mode shapes of the rotor blades

unsteady pressures so pre-stress effects are neglected. For the mechanical damping a damping rate of 0.0011 was determined from an experimental modal analysis, the aerodynamic damping was not considered.

Results

The trailing-edge thickness is chosen as the variable for the forced-response analysis. In the present study, three different trailing-edge thicknesses are investigated. Compared to the reference geometry, the trailing-edge is made 30% thinner in the first case, in which these thinner stator vanes alternate with the reference geometry (see Fig. 13). For the two other cases, the thin stator vanes are kept, while for the alternating stator vanes, the trailing-edge thickness is increased by 30% and 60% compared to the reference stator vanes, respectively.

For the data analysis, the unsteady pressures are first transformed to the frequency domain as outlined in the process described above (Fig. 9). The first three harmonics of the BPF of 3750 Hz are obtained plus the frequency of 1875 Hz, which is caused by the alternating stator vanes. This operating point is chosen because the Campbell diagram for this machine (see Fig. 12) predicts a resonance with the second eigenfrequency of the rotor blades for the excitation by the alternating stator variation. By exciting the 2^{nd} blade mode the computational effort was reduced compared to exciting the 1^{st} blade mode, which would have required a larger sector to be modeled in the CFD.

Figure 10 shows the point on the blade where the nodal displacement is evaluated at the trailing-edge (TE). This is the location of the maximum displacement. The three cases of stator variance in the stator vane thickness lead to a significant increase in vibration amplitude as depicted in Fig.13. A variation of -30% trailing-edge thickness increases the superimposed amplitude response of the downstream rotor blade row by a factor of three and half compared to the reference case with unaltered stators. For second i.e. the $\pm$30% case, the amplitude of the response more than doubles to seven and half times that of the reference amplitude. In the case of the third configuration, the amplitude increases further by a factor of fourteen. This characteristic is also detected at the frequency of 1875 Hz. The variance-induced excitation does not lead to a significant increase of the response amplitudes at the harmonics of the BPF, which are off-resonance in this operating point.

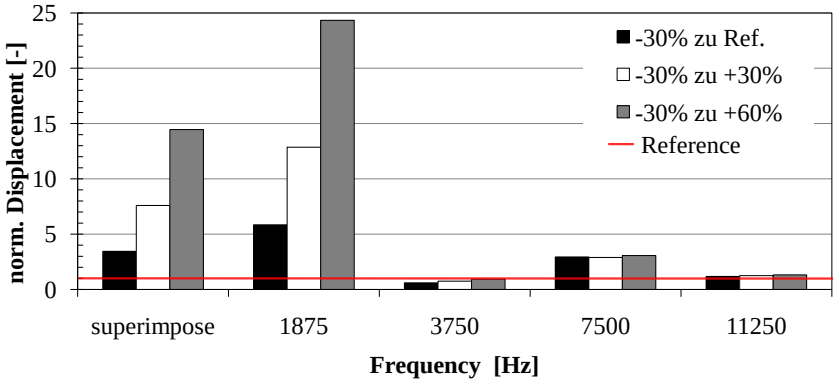

Figure 13: Normalized displacement at rotor tip trailing-edge for alternating trailing-edge variance on stator blades.

CONCLUSIONS and OUTLOOK

In the present paper, typical geometrical variances of turbine blades induced by regeneration are investigated. Significant deviations of geometrical parameters are found and transferred to the vanes of a model air-turbine. The influence of the deviations on the aerodynamic are analysed by steady CFD simulations. This analysis indicates a high influence on the total pressure-loss coefficient and on the outlet flow angle of the vanes.

The forced-response analysis shows that the vibration amplitudes of the low eigenfrequencies of the downstream rotor blades are three and a half times higher due to a 30% change of the trailing-edge thickness of alternating upstream stator vanes. A larger variation leads to a further increase in amplitude. Thus, the regeneration-induced variances have a significant impact on the low engine-order excitation and must be considered when defining the tolerance of the regeneration process.

Future steps will include an investigation of the influence of other geometrical variations in the stator vane on the low engine-order excitation also using the forced response analysis. The numerical results will be verified with experiments in the axial air-turbine.

ACKNOWLEDGEMENTS

The authors kindly thank the German Research Foundation (DFG) for the financial support to accomplish the research project C4 “Regeneration-induced Variance of Aeroelastic Properties of Turbine Blades” within the framework of the Collaborative Research Center (SFB) 871. Furthermore the authors want to thank David Feldmann and Adrian Polaczek for the contribution made with their project theses.

References

Bammert, K., Sandstede, H., 1976. Influence of manufacturing tolerances and surface roughness of blades on the performance of turbines. Journal of Engineering for Power 1976, 29–36.

Bréard, C., Green, J., Imregun, M., 2003. Low-engine_order excitation mechanisms in axial-flow turbomachinery. Journal of Propulsion and Power 2003 (Vol. 19), 704–712.

Chiang, H., Kielb, R., 1993. An Analysis System for Blade Forced Response. Journal of Turbomachinery 115, 762–770.

Di Mare, L., Imregun, M., Smith, A., Elliott, R., 2007. A numerical study of high pressure turbine forced response in the presence of damaged nozzle guide vanes. Aeronautical Journal Vol. 111 (No. 3177), 751–757.

Drewczynski, M., Solinski, M., Rzadkowski, R., 2012. A comparison of two load transferring methods in an unsteady one-way fluid-structure interaction analysis. Proceedings of ASME Turbo Expo 2012, June 11-15, Copenhagen, Denmark (GT2012-69543).

Förstching, H., 1994. Aeroelastic stability of cascades in turbomachinery. Progress in Aerospace Sciences 30 (3), 213–266.

Goulos, I., Zachos, P., Kalfas, A., Pilidis, P., 2009. Turbine performance effects from geometry variations between manufacturing components and design intent. ISABE-2009-1260.

Henke, M., Guendogdu, Y., Seume, J., Siewert, C., Panning, L., Wallaschek, J., 2008. Unidirectional coupled aerodynamic and structural mechanics analysis of a turbine blading. Proceedings of IMechE 2008, 171–184.

Lange, A., Vogeler, K., Schrapp, H., Clemen, C., 2008. Ein parametrisches modell für verdichterschaufeln zur abbildung von geometrischen abweichungen in der numerischen simulation. 1. Dresdner-Probabilistik-Workshop.

Meyer, M., Parchem, R., Davison, P., 2011. Prediction of Turbine Rotor Blade Forcing due to in-service Stator Vane Trailing Edge Damage. Proceedings of ASME Turbo Expo 2011, June 6-11, Vancouver, Canada (GT2011-45204).

Petrov, E., Di Mare, L., Hennings, H., Elliott, R., 2010. Forced response of mistuned bladed disks in gas flow: A comparative study of predictions and full-scale experimental results. Journal of Engineering for Gas Turbines and Power 132 (Vol. 132).

Torre, D., Vázquez, R., Armananzas, L., Partida, F., Garcia-Valdecasas, G., 2012. The effect of airfoil thickness on the efficiency of lp turbines. Proceedings of ASME Turbo Expo 2012, June 11-15, Copenhagen, Denmark (GT2012-68556).

Traupel, W., 1982. Thermische Turbomaschinen, 3rd Edition. Vol. 2. Springer.

Zachos, P., Kalfas, A., 2010. Analysis of turbine performance degradation effects due to geometry variations between actual components and design intent. The Aeronautical Journal 114 (159), 569–577.